Available online at www.sciencedirect.com

SCIENCE DIRECT®

Earth and Planetary Science Letters 225 (2004) 347–363

EPSL

www.elsevier.com/locate/epsl

Fluid expulsion from the Dvurechenskii mud volcano (Black Sea) Part I. Fluid sources and relevance to Li, B, Sr, I and dissolved inorganic nitrogen cycles

Giovanni Aloisi[a,*], Manuela Drews[a], Klaus Wallmann[a], Gerhard Bohrmann[b]

[a] *GEOMAR Research Center, Wischhofstr. 1-3, D-24148 Kiel, Germany*
[b] *Research Center for Ocean Margins, University of Bremen, Post Box 330 440, D-28334 Bremen, Germany*

Received 5 December 2003; received in revised form 2 June 2004; accepted 1 July 2004

Editor: E. Boyle

Abstract

Significant sediment–ocean chemical fluxes are produced by the expulsion of sedimentary fluids at continental margins. Although such fluxes could play a role in global geochemical cycles, few quantitative estimates of their global, or even regional, significance exist. We carried out a pore water geochemical study of fluids expelled from the Dvurechenskii mud volcano (DMV) in the Black Sea, with the aim of understanding the role played by mud volcanoes in Black Sea geochemical cycles. The DMV is presently expelling highly saline fluids particularly enriched in geochemically important species such as Li^+ (1.5 mM), B (2.17 mM), Ba^{2+} (0.57 mM), Sr^{2+} (0.79 mM), I (0.4 mM) and dissolved inorganic nitrogen (DIN) (22 mM). A combination of geochemical indicators shows that this geochemical signature was acquired via organic matter and silicate alteration processes in the subsurface down to 3-km depth and near-surface gas hydrate formation. We used a simple transport model to estimate the benthic fluxes of these solutes at the DMV. Our results show that the DMV is expelling fluids at a rather low seepage rate (8–25 cm $year^{-1}$) resulting in a total water flux of 9.4×10^{-5} km^3 $year^{-1}$. This gentle regime of fluid expulsion results in Li^+, B, Sr^{2+}, I and DIN fluxes between 3.8×10^4 and 2.1×10^6 mol $year^{-1}$. Surface biogeochemical processes affect the benthic fluxes of Ba^{2+} such that the deep Ba^{2+} flux is completely consumed through the precipitation of authigenic barite ($BaSO_4$) in surface sediments. The Black Sea I cycle is likely to be affected by mud volcanism, if the 50 known Black Sea mud volcanoes share the rather sluggish activity of the DMV. Mud volcano fluxes of Li, B, Sr and DIN, instead, are too small to affect Black Sea geochemical cycles. On a global scale, mud volcanism could play a role in the marine cycles of Li, B, Sr, I and DIN if current estimates of mud volcano abundance are correct.
© 2004 Elsevier B.V. All rights reserved.

Keywords: mud volcano; Black Sea; cold seeps; fluid sources; chemical fluxes

* Corresponding author. Current address: Laboratoire de Paléoenvironments et Paléobiosphère, Université Claude-Bernard, Lyon I, 2, rue Dubois, 69622 Villeurbanne, Cedex, France.
E-mail address: Giovanni.Aloisi@univ-lyon1.fr (G. Aloisi).

0012-821X/$ - see front matter © 2004 Elsevier B.V. All rights reserved.
doi:10.1016/j.epsl.2004.07.006

1. Introduction

The expulsion of sedimentary fluids at continental margins generates significant water and chemical fluxes [1–3]. Fluid–sediment and fluid–rock interactions during sediment burial alter pore fluid chemistry considerably, such that the expelled fluids can be chemically very different from seawater. Diagenetic processes involving organic matter degradation [4], barite dissolution [5,6], desorption/transformation reactions involving clay minerals [7–9] and high-temperature reactions with volcanic ashes and oceanic or continental crust [2,10,11] concentrate geochemically important species such as Sr^{2+}, Ba^{2+}, Li^{+}, B, I and dissolved inorganic nitrogen (DIN) in pore fluids with progressive burial. Thus, the expulsion of sedimentary fluids is a potential source in the marine geochemical cycles of these species.

Estimating the importance of cold seep Sr^{2+}, Ba^{2+}, Li^{+}, B and I fluxes is important because their geochemical cycles are applied to solve a large number of geologic problems. The Li and B cycles, for example, are used to reconstruct seawater pH evolution in time and to investigate mid-ocean ridge hydrothermalism and oceanic crust alteration processes [12–15]; the marine Ba cycle is applied in a number of paleo-oceanographic investigations such as the reconstruction of paleoproductivity and ocean circulation [16–19]; the Sr cycle is central in understanding how carbonate deposition, chemical weathering and hydrothermal activity have influenced earth's climate in the geological past [20]; the I cycle is potentially useful to investigate the recycling of sedimentary fluids in fore-arc areas [21].

Much of the difficulty in assessing cold seep elemental fluxes lies in the scarcity of available flux measurements. Some indications exist that past and/or present cold seep fluxes of Li, B and Ba may be relevant to the regional or global geochemical cycles of these species [22–27]. Recent estimates of cold seep Ba fluxes obtained with benthic chambers and biogeochemical modeling, for example, show that the cold seep Ba source likely affects Ba cycling in the Santa Barbara basin [28] and in the Derugin basin of the Sea of Okhotsk [27]. You et al. [22,23] observed extreme B and Li enrichments (3 and 0.8 mM, respectively) in sedimentary fluids of the Nankai and Barbados accretionary prisms. By multiplying the concentration of the diagenetically enriched solutes by the global cold seep water discharge of 1 $km^3\ year^{-1}$ [29,30], these authors obtain global B and Li flux estimates which are significant to the global cycles of these elements. The importance of the cold seep Sr, I and DIN fluxes to the marine cycles of these species, instead, has not been investigated yet.

Seepage of sedimentary fluids occurs diffusively, canalized through high-permeability sedimentary or tectonic pathways, or in association with major pathways of mud expulsion like mud diapirs and mud volcanoes [31,32]. Because mud volcanoes expel fluids originating typically from several kilometres depth [11,31,33], they are preferential conduits through which deep, chemically enriched fluids can reach the ocean. Mud volcanoes offer a unique possibility to measure chemical fluxes from relatively large portions of the seafloor. A recent estimate proposes that 10^3 to 10^5 submarine mud volcanoes exist worldwide [34]. Estimates of Li, B, Ba, Sr, I and DIN fluxes based on such mud volcano abundances have not been undertaken yet.

We present a first evaluation of how the expulsion of diagenetically altered fluids from mud volcanoes affects the global and Black Sea geochemical cycles of Li^{+}, B, Ba^{2+}, Sr^{2+}, I and DIN. We investigated fluids expelled from the Dvurechenskii mud volcano (DMV), located in the Sorokin Trough of the Black Sea, using a variety of geochemical indicators to constrain the source depth and the diagenetic processes controlling their chemical composition. A simple transport model is used to estimate the fluid seepage rate and, from this, to calculate benthic fluxes. We paid particular attention to how biogeochemical process in surface sediments affect Ba^{2+} and Sr^{2+} fluxes. We then make conservative estimates of the volcano fluxes of these species to the Black Sea water column and compare these estimated fluxes with the major inputs of Sr^{2+}, Ba^{2+}, Li^{+}, B, I and DIN to the Black Sea from the Danube River and the Mediterranean. Finally, we use the estimated worldwide abundance of mud volcanoes to produce an order-of-magnitude estimate of the global mud volcano flux of these species. In a companion paper, we investigate the methane flux from the

DMV and its relevance to the Black Sea methane cycle [35].

2. Study area

2.1. Mud volcanism in the Sorokin Trough

The Sorokin Trough is located SE of the Crimean peninsula (Fig. 1) and is considered to be the foredeep of the Crimean Alpine range [36]. It was formed in Oligocene/Early Miocene times and forms a large, SW–NE-oriented depression 150-km long and 50-km wide [37]. This area is subject to a N–S-oriented compressive regime generated by the northwards motion of the buried Tetyaev and Shatskii rises [37]. These structural highs act as rigid buttresses against which clays of the Maikopian formation (Oligocene–Lower Miocene) are deformed, become overpressured and rise diapirically [38]. As a result, the sedimentary succession in the Sorokin Trough is pierced by numerous diapiric ridges which have roots several kilometers deep and are bathymetrically expressed as SE–NE bathymetric highs [39]. Numerous mud volcanoes are located on the culmination of these diapiric ridges (Fig. 1), suggesting a genetic link between mud diapirism and mud volcanism [37,40,41].

2.2. The Dvurechenskii mud volcano (DMV)

The DMV lies on the culmination of an E–W-trending sector of a diapiric ridge (Fig. 1). A multichannel seismic survey across the DMV shows that the underlying diapiric intrusion is most probably fault-controlled and extends below the maximum penetration of the seismic data (~3.5 km; [41]). Morphologically, it is a round, flat-topped elevation 800 m in diameter and 80 m in height. Echosounder and deep-tow side scan sonar surveys indicate that the uppermost 30 m are composed of acoustically homogeneous sediments [41]. These surveys imaged mud flows that originate from the summit of the DMV and extend downslope along its flanks. During a deep-tow TV survey, patches of white bacterial mats a few decimeters across were observed on the summit of the DMV, pointing to ongoing or recent fluid emission activity [40].

We studied five gravity cores (TGC-2, -3, -5, -7 and -8) and three short cores from multicorers (MIC-3, MIC-4 and MIC-5) obtained from the summit of the DMV during the MARGASH cruise of the *R/V Meteor* in 2001 (Fig. 2, Table 1; [39]). All cores are

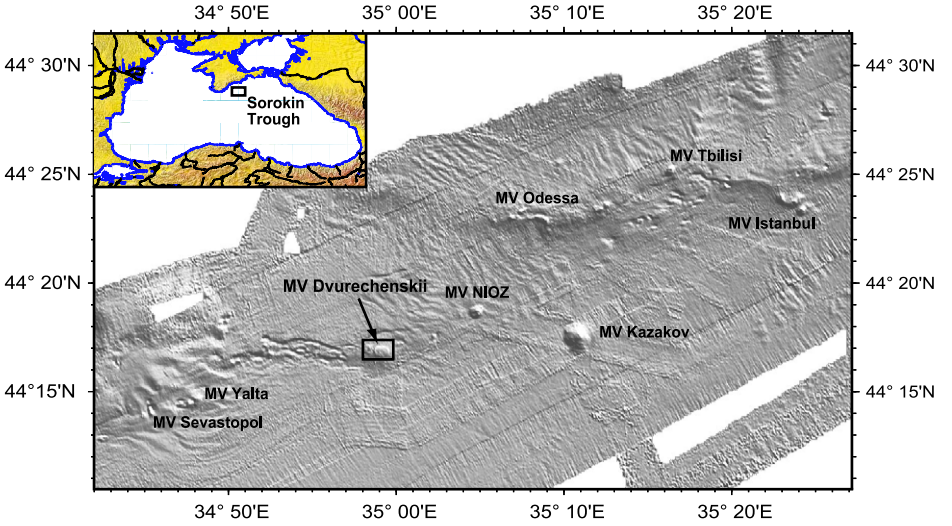

Fig. 1. Side scan sonar image of mud volcanoes in the Sorokin Trough, SE of the Crimean Peninsula. Most mud volcanoes (MV) lie on the culmination of an ENE–WSW morphological ridge, which is the bathymetric expression of diapiric ridges formed in the compressional regime between the Tetyaev and Shatskii Rises. The detail of the Dvurechenskki mud volcano (rectangle) is enlarged in Fig. 2.

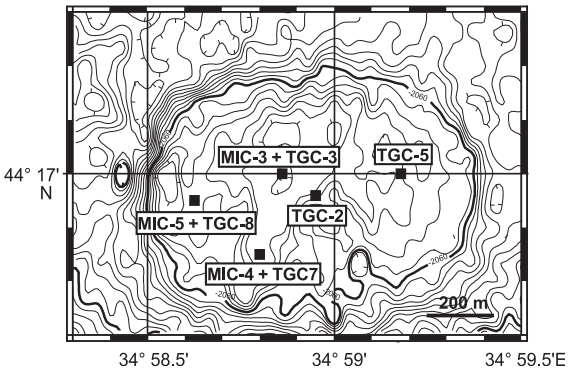

Fig. 2. Bathymetric map of the Dvurechenskii mud volcano which is a flat-topped feature. The position of five piston cores and three short cores included in this study is marked. The thick isobath is at 2060-m depth. Fine isobaths are at 5-m depth intervals.

composed of very fluid, dark grey mud which contains millimeter- to centimeter-sized rounded rock clasts. Most clasts are mudstones probably originating from the Maikopian formation (Ivanov, personal communication). This matrix-supported sediment has been described from other mud volcanoes and is termed 'mousse-like mud breccia' [42]. Small gas hydrate crystals dispersed in the mud breccia were observed in all cores from the DMV. Lenticular gas hydrates were recovered only in core TGC-2. A 2-cm-thick layer of pelagic sediments is present at the very top of most cores, suggesting that some time has passed since the last mud expulsion event. The flat shape of the DMV summit is probably a consequence of the high fluidity of the expelled mud which favours the development of gentle slopes [43]. Similar mud volcanoes have been described from the Barbados Accretionary Prism where they are associated with gas hydrates, high fluid flow rates and gas emissions [31].

3. Methods

3.1. Sampling and chemical analysis

Coring was carried out with a 6-m-long gravity corer (TGC) and a 45-cm-long multicorer (MIC). After recovery, gravity cores were split on deck and rapidly subsampled. Sediment from the multicorer was cut into slices in the on-board laboratory, which was kept at 4 °C. Pore water extraction was carried out at 4 °C in the on-board laboratory.

Pore waters were analyzed on board for dissolved ammonia (NH_4=[NH_4^+]+[NH_3]) and sulfide (H_2S=[H_2S]+[HS^-]+[S^{2-}]) using standard photometric procedures [44]. Total alkalinity (TA) was determined by titration immediately after pore water separation [45]. The remaining pore waters were later analyzed in the shore-based laboratory for dissolved anions (SO_4^{2-}, Cl^-, I^-, Br^-) and dissolved elements (Na^+, K^+, Li^+, Mg^{2+}, Ca^{2+}, Sr^{2+}, Ba^{2+}, B (=[$B(OH)_3$]+[$B(OH)_4^-$]), Si (=[H_4SiO_4]+[$H_3SiO_4^-$])) using ion chromatography and optical ICP, respectively. Subsamples for dissolved element analyses (ICP) were acidified immediately after squeezing to prevent further $CaCO_3$ precipitation. Sediment pH was measured in the 4 °C laboratory with a pH electrode calibrated using a buffer prepared in artificial seawater [46]. The porosity was calculated from the water content assuming a dry solid density of 2.65 g cm^{-3}. The oxygen isotope composition of pore water was measured by mass spectrometry at the Laboratory GCA, Sehnde, Germany. All analytical procedures applied on board and in our GEOMAR laboratories are documented in detail at: http://www.geomar.de/zd/labs/laboreumwelt/Meth_englisch.html.

Table 1
Sampling sites included in this study

Core[a]	Region of DMV	Latitude (°N)	Longitude (°E)	Water depth (m)
TGC-2	DMV summit, centre	44°16.96′	34°58.95′	2074
MIC-3	DMV summit, centre	44°16.99′	34°58.81′	2070
TGC-3	DMV summit, centre	44°17.00′	34°58.86′	2071
TGC-5	DMV summit, E	44°17.00′	34°59.18′	2075
MIC-4	DMV summit, SW	44°16.88′	34°58.80′	2085
TGC-7	DMV summit, SW	44°16.85′	34°58.80′	2087
MIC-5	DMV summit, W	44°16.97′	34°58.61′	2089
TGC-8	DMV summit, SW	44°16.95′	34°58.63′	2087

[a] MIC—minicorer; TGC—thermistor gravity corer.

3.2. Setup of the numerical transport model

Rates of upward fluid flow at the DMV were determined applying a transport model to the inert tracer chloride dissolved in the pore fluids of short cores MIC-3, MIC-4 and MIC-5. The model considers molecular diffusion and advection of dissolved chloride and is based on the following differential equation:

$$\Phi\frac{\partial[\mathrm{Cl}^-]}{\partial t}=\frac{\partial\left(\Phi\frac{D_{\mathrm{Cl}}}{\Theta^2}\frac{\partial[\mathrm{Cl}^-]}{\partial x}\right)}{\partial x}-\Phi v\frac{\partial[\mathrm{Cl}^-]}{\partial x} \quad (1)$$

where t is time, x is sediment depth, $[Cl^-]$ is the concentration of dissolved chloride, D_{Cl} is the molecular diffusion coefficient of Cl^-, Φ and Θ are sediment porosity and tortuosity, and v is the velocity of vertical fluid flow. The unknown velocity rate is determined by fitting the model to the data. The effect of sedimentation on the advection rate of fluids is not considered since advection of fluids at cold seeps is dominated by seepage, rather than by burial [47].

Sediment porosity changes with depth due to sediment compaction. The depth profile is approximated using the following exponential function [48]:

$$\Phi=\Phi_{\mathrm{f}}+(\Phi_{\mathrm{i}}-\Phi_{\mathrm{f}})e^{-px} \quad (2)$$

where the parameter values for Φ_f (porosity at infinite depth), Φ_i (porosity at zero depth), and p (attenuation coefficient for the exponential decrease of porosity with depth) are determined by fitting the porosity model to the corresponding porosity data.

Sediment tortuosity is calculated from porosity using the following empirical relation [49]:

$$\Theta^2=1-\ln\left(\Phi^2\right) \quad (3)$$

Boundary conditions were defined at the sediment surface (x=0) and at the base of the model column (x=L=26–38 cm), corresponding to the maximum depth from which the pore water was collected in the different short cores. The model was run into steady state starting from arbitrary initial conditions. Due to the high flow velocities, steady state was usually attained within a few years. MATHEMATICA version 4.1 was used to implement the model.

Table 2 summarizes the parameter values which were used for the modeling of upward fluid flow in the short core sediment columns.

Table 2
Parameter values used in the modeling

Parameter	Symbol	Value
Length of the model column (cm)	L	26–38
Average surface sediment temperature (°C)	T	10
Chloride concentration at zero depth (mM)	Cl_0	350
Chloride concentration at depth L (mM)	Cl_L	760–815
Molecular diffusion coefficient of chloride at T (cm^2 $year^{-1}$)	D_{Cl}	441
Sedimentation rate at infinite depth (cm $year^{-1}$)	w_f	0.03

4. Results

The concentration profiles of Na^+, Cl^-, Mg^{2+}, SO_4^{2-}, K^+, Si, B, Li^+, Ca^{2+}, Sr^{2+}, Ba^{2+}, NH_4, H_2S, Br^- and I^-, and profiles of $\delta^{18}O_{H2O}$, TA and the Br^-/Cl^- ratio at sites TGC-2, -3, -5, -7 and -8 are showed in Fig. 3. The concentration profiles of Na^+, Cl^-, Mg^{2+}, SO_4^{2-}, K^+, Si, B, Li^+, Ca^{2+}, Sr^{2+}, Ba^{2+}, Br^- and I^-, and the $\delta^{18}O_{H2O}$ profile at sites MIC-3, -4, and -5 are presented in Fig. 4. The results of applying the transport model introduced in Section 3.2 to the Cl^- profiles of short cores MIC-3, MIC-4 and MIC-5 are given in Fig. 5.

5. Discussion

5.1. Seepage of hypersaline fluids at the DMV

The geochemical profiles obtained from gravity cores are remarkably similar from site to site (Fig. 3). Between roughly 50–100-cm depth and the bottom of the cores, solute concentrations are constant with depth and deviate significantly from bottom water values. In the upper 50–100 cm of sediments, steep concentration gradients exist between the lower part of cores and bottom water concentrations. The short cores taken in close proximity of gravity cores (Fig. 2) provide a detailed picture of the upper 40 cm of the gradients observed in gravity cores (Fig. 4). Thus, most solute concentration profiles show the same trends seen in the upper part of the gravity cores. In addition, the high sampling resolution used in the short cores highlights the concave downward shape of most profiles, a feature which indicates advective transport of fluids from below. Confirming this observation, the best fit of the

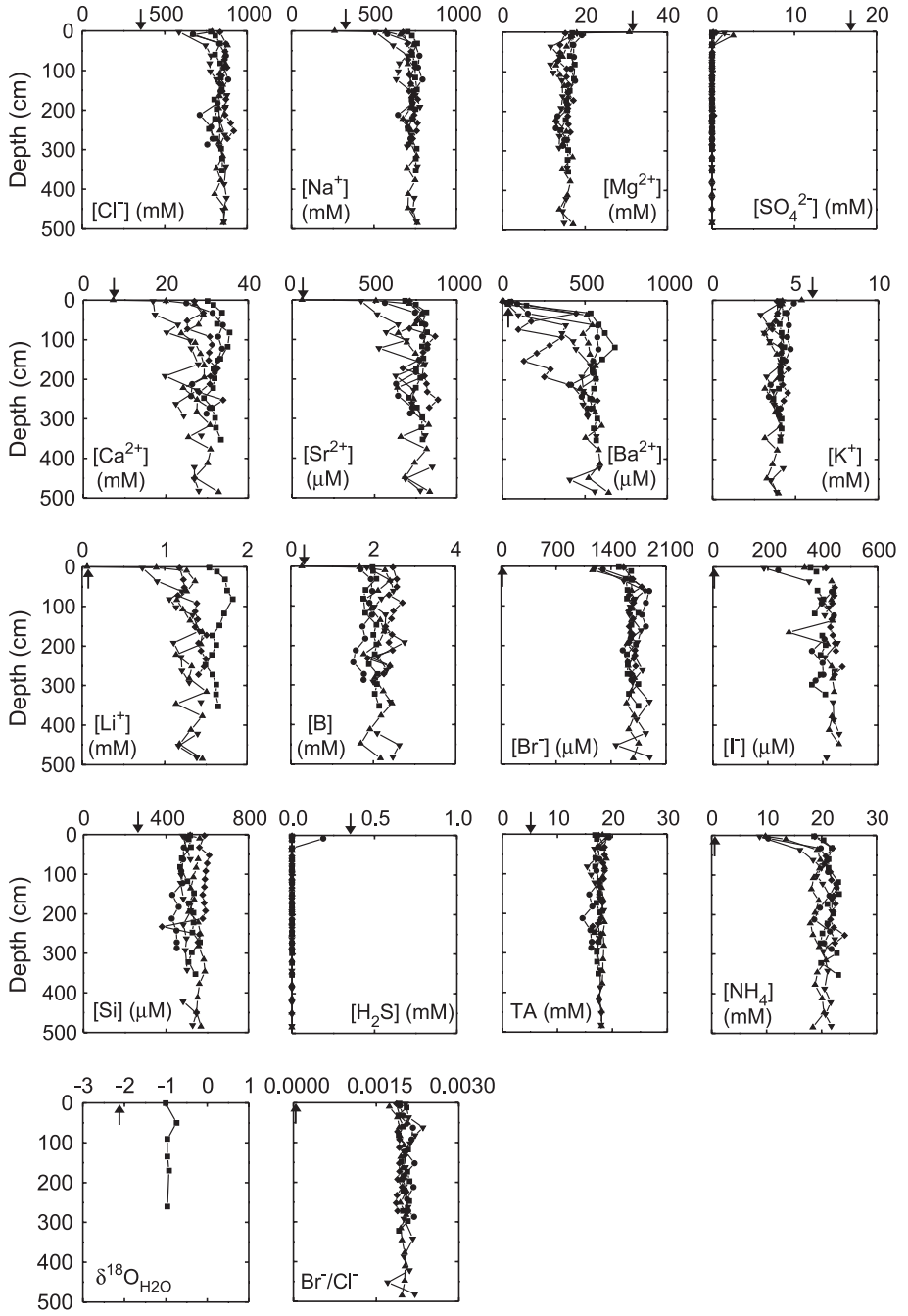

Fig. 3. Chemical and isotopic composition of pore fluids from gravity cores TGC-2 (■), -3 (◆), -5 (●), -7 (▲) and -8 (▼). Arrows indicate the composition of Black Sea bottom waters.

model Cl^- curves produced with the transport model to the Cl^- data was obtained imposing an advection velocity varying from 8 cm $year^{-1}$, at the station farthest from the centre (core MIC-5), to 25 cm $year^{-1}$, at the centre of the DMV summit (core MIC-3). Thus, the DMV is actively emitting fluids.

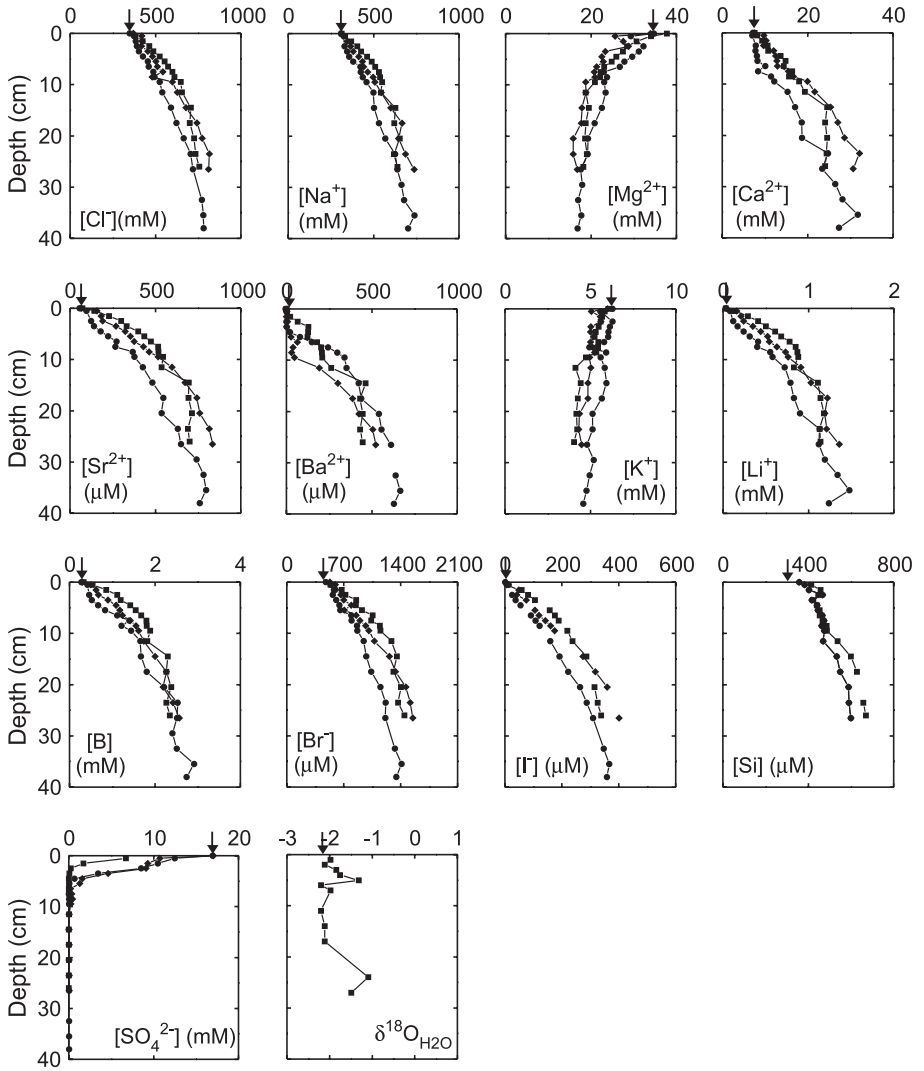

Fig. 4. Chemical and isotopic composition of pore fluids from short cores MIC-3 (■), -4 (◆) and -5 (●). Arrows indicate the composition of Black Sea bottom waters.

The constrained seepage rates fall in the lower end of the range of seepage rates most commonly found at cold seeps (0–1000 cm year^{-1}; [47,50]). Although the seepage rates at the DMV are not extremely high, they have a strong impact on pore water chemical profiles in the uppermost meters of the DMV sediments. Luff and Wallmann [47] have shown that when seepage rates exceed a few centimeters per year, diffusive exchange between bottom waters and sediment pore fluids is limited to the upper few centimetres of sediments. At greater depths, solute concentrations are dominated by advective transport of fluids from below. Thus, the composition of fluids below 100 cm in the gravity cores from the DMV is representative of that of the deep fluids, possibly modified by diagenetic processes during transit to the surface. The composition of the DMV fluids, calculated as the average composition of pore fluids from all cores below 2-m depth, is shown in Table 3. The fluids expelled from the DMV contain 50 g/l of dissolved salts and are thus hypersaline. Concentrations of Cl^-, Br^-, I^-, Ca^{2+}, Na^+, Ba^{2+}, Li^+, Sr^{2+}, B, NH_4 and TA are considerably

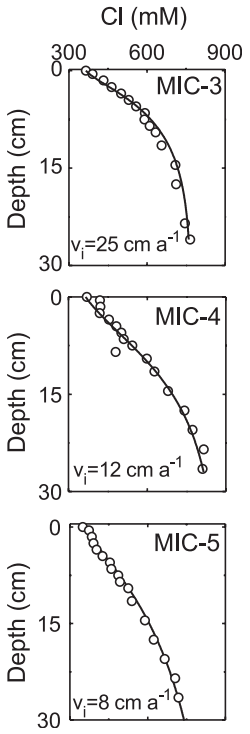

Fig. 5. Measured (circles) and model (curves) concentration profiles of Cl^- in the surface sediments of the Dvurechenskii mud volcano (short cores MIC-3, MIC-4 and MIC-5). The short cores are positioned at increasing distance from the centre (MIC-3) to the rim (MIN-5) of the Dvurechenskii summit.

higher than in bottom waters. In particular, the ions Cl^-, Na^+, Ca^{2+}, Sr^{2+} and B are 2 to 12 times more concentrated in the DMV fluids than in bottom waters. Extreme enrichments are observed for Li^+ (~24 times bottom waters), I^- (~110 times bottom waters) and Ba^{2+} (~1000 times bottom waters). Concentrations of Si and K^+, instead, are comparable to bottom water values while Mg^{2+} is depleted in the DMV fluids. SO_4^{2-} and H_2S are nearly absent below 1-m depth. $\delta^{18}O$ values, at a constant −1‰ vs. SMOW, are about 1‰ heavier than modern Black Sea bottom waters.

5.2. Genesis of the DMV fluids

Fontes and Matray [51] show that halite precipitates during the evaporation of seawater when a Cl^- concentration of ~5000 mM is attained. The Cl^- concentration of the Dvurechenskii fluid is 810 mM. Thus, should the high salinity of the Dvurechenskii fluid be due to evaporation, Cl^- will have behaved conservatively during the evaporation-diagenesis path. We can therefore use solute/Cl^- ratios in the Dvurechenskii fluid as indicators of diagenesis-induced chemical alteration of pore fluids. In Table 3 we compare solute/Cl^- ratios of the mud volcano fluid with the same ratios in modern Black Sea water. Larger solute/Cl^- ratios for Ca^{2+}, B, Br^-, Sr^{2+}, Si, I^-, Ba^{2+}, Li^+, TA and NH_4 in the Dvrurechenskii fluid compared to Black Sea water indicate that diagenetic processes resulted in a net production of these solutes. K^+/Cl^- and Mg^{2+}/Cl^- ratios are smaller in the mud volcano fluid than in Black Sea water, indicating net consumption of K^+ and Mg^{2+}, while the Na^+/Cl^- ratios of the two fluids are comparable, indicating either that Na^+ has behaved conservatively or that diagenetic processes resulted in no net loss or production of Na^+.

5.2.1. Organic matter degradation processes

The oxidation of organic matter using sulfate increases total alkalinity through production of HS^-

Table 3
Comparison between Dvurechenskii fluid and Black Sea water chemistry

Solute	Black Sea[a]	DMV fluid[b]	([Sol.]/[Cl^-])$_{BS}$[c]	([Sol.]/[Cl^-])$_{DMV}$[d]
Cl^-	355 mM	835 mM	1	1
Na^+	300 mM	730 mM	0.85	0.87
Mg^{2+}	34.8 mM	18.3 mM	9.7×10^{-2}	2.2×10^{-2}
SO_4^{2-}	16.8 mM	0 mM	4.7×10^{-2}	0
Ca^{2+}	7.5 mM	29.8 mM	2.1×10^{-2}	3.5×10^{-2}
K^+	6.3 mM	4.3 mM	1.8×10^{-2}	5.0×10^{-3}
B	0.27 mM	2.17 mM	7.6×10^{-4}	2.6×10^{-3}
Br^-	4.9 μM	1.74 mM	1.4×10^{-5}	2.1×10^{-3}
Sr^{2+}	57.6 μM	0.79 mM	1.6×10^{-4}	9.5×10^{-4}
Si	0.32 mM	0.54 mM	9.0×10^{-4}	6.5×10^{-4}
I^-	0.56 μM	0.34 mM	1.6×10^{-6}	4.1×10^{-4}
Ba^{2+}	446 mM	0.57 mM	1.3×10^{-6}	6.8×10^{-4}
Li^+	16.8 μM	1.5 mM	4.7×10^{-5}	1.8×10^{-3}
TA	4.3 mM	18.3 mM	1.2×10^{-2}	2.2×10^{-2}
NH_4	46.2 μM	22 mM	1.0×10^{-4}	2.6×10^{-2}
H_2S	0.37 mM	0 mM	1.0×10^{-3}	0
$\delta^{18}O$	−1.65‰	−0.9‰	–	–

[a] Black Sea bottom water sampled in the Sorokin Trough during cruise M52-1.
[b] Composition of Dvurechenskii fluids calculated as average concentration in the lower part of the DMV gravity cores.
[c] [Solute]/[Cl^-] ratio in Black Sea bottom waters.
[d] [Solute]/[Cl^-] ratio in Dvurechenskii fluids.

and HCO_3^-, and releases NH_4, Br^- and I^- [11,52,53]. The Dvurechenskii fluids are free of sulfate and are significantly enriched in NH_4, Br^-, I^- and alkalinity (Table 3). In addition, the Br^-/Cl^- ratio is considerably higher in the Dvurechenskii fluids than in Black Sea waters, confirming that extensive organic matter degradation has taken place. The absence of sulfide is probably due to sulfide mineral precipitation at depth.

5.2.2. Sources of Sr and Ba

Ba is present in marine sediments mostly as 'bio-barite' ($BaSO_4$) formed in sedimentary basins overlain by biologically highly productive water columns. Sr can substitute effectively for Ca in carbonates and for Ba in barite [54,55]. Thus, Sr and Ba are susceptible of being redistributed between fluids and authigenic phases during precipitation/dissolution processes involving these minerals [6,54]. Barium dissolved in cold seep fluids is thought to originate from the dissolution of barite below the depth of sulfate depletion of marine sediments [24]. A deeper source of Ba^{2+} and Sr^{2+} possibly is the alteration of sediment-bearing basement rocks, because these elements are abundant in sedimentary material. It is plausible that the elevated Ba^{2+} content of the Dvurechenskii fluids derives from dissolution of bio-barite. However, this process cannot be the sole source of Sr^{2+}, given that the Sr/Ba ratio in bio-barite is only 0.032 [55]. Elevated Sr^{2+} concentration in fluids expelled from mud volcanoes of the Barbados accretionary prism, however, is interpreted as due to Sr^{2+} release during the recrystallization of carbonates [11], and it is possible that also this process is taking place in Black Sea sediments.

5.2.3. Silicate alteration processes and source depth

The alteration of silicate materials affects the pore fluid concentration of several species like Ca^{2+}, Mg^{2+}, Li^+, Na^+, B, K^+ and Sr^{2+}, producing a pore fluid chemical signature which depends on the temperature and on the nature of the alteration minerals formed [10,11,56]. The best known diagenetic process involving silicates in marine sediments is the alteration of volcanic ash [11,57,58]. In addition to consuming water and concentrating ^{18}O in the diagenetic clay minerals, this process results in the depletion of Mg^{2+}, K^+ and Na^+ and in the enrichment in Ca^{2+} of the diagenetic fluids:

$$\text{volcanic ash} + Mg^{2+} + K^+ + Na^+ + H_2O \rightarrow \text{smectite} + Ca^{2+} \quad (4)$$

The Dvurechenskii fluids are considerably depleted in Mg^{2+} and K^+ and enriched in Ca^{2+} (Table 3), which is consistent with volcanic ash alteration. Because the nature of the sediments from which the fluids originate and through which they migrate before being expelled is not known, it is not possible to identify the nature of the silicates. Drilling during DSDP Leg 42A failed to find volcanic ash deposits in the upper 600 m at Site 379 in the central Black Sea abyssal plain. However, we cannot exclude that volcanic ash deposits are present in deeper sedimentary intervals and that volcanic ash alteration is going on there. Alternatively, the observed chemical shifts are produced by the submarine weathering of detrital silicate minerals. This process has been recently described from Black Sea sediments where it is driven by the low pH and high P_{CO2} of pore waters [59].

However, the Dvurechenskii fluids are significantly enriched in Li and B, suggesting that diagenetic processes resulted in a net source of Li and B. Since the low temperature silicate alteration reaction described above consumes Li and B, this implies the presence of an important diagenetic source of these elements for the Dvurechenskii fluids. During progressive burial Li and B are released to pore fluids through desorption [9,60]. Li and B are further released starting from T~50 to 60 °C from pelagic sediments [7–9] and following clay mineral dehydration/transformation processes [61,62].

We estimated the maximum temperature experienced by the Dvurechenskii fluids by applying the empirical lithium and magnesium geothermometer [11,63]. The concentration of Li^+ and Mg^{2+} in the deepest gravity core samples was used to calculate the equilibrium temperature according to the following formula [11,63]:

$$t\ ^\circ\mathrm{C} = \frac{2200}{\log\left(\frac{\sqrt{\mathrm{Mg}}}{\mathrm{Li}}\right) + 5.47} - 273 \quad (5)$$

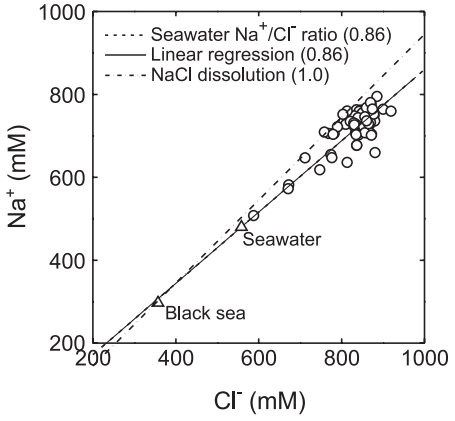

Fig. 6. Na^+/Cl^- relationship in fluids sampled with gravity cores from the summit of the Dvurechenskii mud volcano. The linear regression through the Dvurechenskii data points extrapolates to average seawater and Black Sea Na^+/Cl^- ratios.

where t is temperature (°C) and Mg and Li concentrations are in mg/l. The resulting temperature range for the Durechenskii fluid is 98 to 103 °C. Considering the regional thermal gradient of 29 °C/km [40], the estimated depth of provenance of the Dvurechenskii fluids is 3 km.

B is often enriched in mud volcanic fluids following clay mineral, and chiefly smectite–illite transformations [25,64]. Because the estimated maximum temperature for the Dvurechenskii fluids falls in the range of temperatures (~60–160 °C) where the smectite–illite clay mineral transformation reaction takes place [29,65], it seems likely that also the Dvurechenskki fluids have been affected by the smectite–illite transformation reaction. Because this reaction produces water, mud volcano fluids containing high amounts of B are also considerably fresher than seawater [64]. The Dvurechenskii fluids, however, couple high B contents to elevated salinity. Thus, a supplementary process that enhances salinity may have contributed in producing the chemical signature of the Dvurechenskii fluid.

5.2.4. Origin of the high salinity and $\delta^{18}O$–Cl^- path

The fluids expelled from the DMV are particularly rich in dissolved Cl and Na (Table 3). Several processes including seawater evaporation, ash diagenesis, gas hydrate formation and dissolution of halite (NaCl) can result in the formation of hypersaline pore fluids [51,58,66–69]. Three of these (evaporation, gas hydrate formation and ash diagenesis) enhance fluid salinity by consuming water, while only halite dissolution increases salinity by addition of dissolved ions. With this in mind, a first discrimination between halite dissolution and the remaining processes can be made based on the Na^+/Cl^- ratio of the expelled fluids. If the elevated Na^+ and Cl^- concentrations of the Dvurechenskii fluid are due to water consumption, then the Na^+/Cl^- ratio should be similar to that of seawater (~0.86), and the data should plot on a line with a slope of ~0.86. If, instead, halite dissolution is providing the Na^+ and Cl^- to fluids, the Na^+/Cl^- ratio should approach unity, since halite provides equal molar amounts of Na^+ and Cl^- upon dissolution. The linear regression through the Dvrurechenskii Na^+ and Cl^- data has a slope of 0.86 (Fig. 6). We can therefore exclude that the Dvurechenskii fluid is a 'secondary brine' formed by the dissolution of halite deposits formed in an evaporitic basin.

Because the water-consuming processes mentioned above produce changes in the oxygen stable isotope composition of water, a further discrimination can be made based on the $\delta^{18}O$ of the expelled fluids. We have plotted the data from the DMV on a $\delta^{18}O$–Cl^- diagram and compared them with calculated fluid $\delta^{18}O$–Cl^- compositions produced by the above processes of water consumption, considering a starting fluid with $\delta^{18}O$ and Cl^- similar to present day Black Sea bottom waters (Fig. 7). The evolution of fluid $\delta^{18}O$ and Cl^- was modelled, assuming a closed

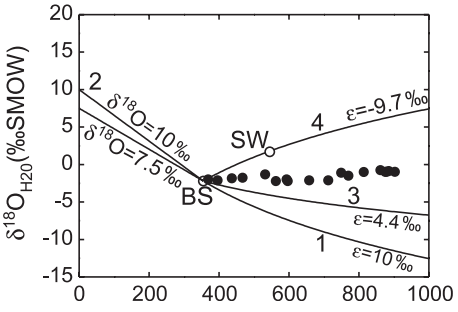

Fig. 7. Comparison of $Cl^-\delta^{18}O$ composition of the DMV fluids with the model closed system evolution of $Cl^-\delta^{18}O$ values during silicate alteration processes (path 1), smectite–illite transformation (path 2), gas hydrate formation (path 3) and evaporation (path 4). BS—Black Sea water; SW—Seawater; DV—Dvurechenskii fluid.

system Raleigh fractionation behaviour, with the following equation:

$$d^{18}O_w([Cl^-]) = d^{18}O_{wi} - \varepsilon \ln\left[\frac{[Cl^-]}{[Cl^-]}\right] \quad (6)$$

where $\delta^{18}O_{wi}$ is the $\delta^{18}O$ of the starting fluid (−2.2‰), $[Cl^-]_i$ is the chloride concentration of the starting fluid (355 mM) and ε is the difference in $\delta^{18}O$ between (a) water vapour and water during evaporation, (b) gas hydrate and water during gas hydrate formation or (c) clay minerals and water during ash diagenesis. Values of ε are taken from Friedman and O'Neil [70] for evaporation at T=25 °C and Matsumoto and Borowski [71] for gas hydrate formation. By analogy to submarine low-temperature alteration of basaltic rocks, the value of ε for ash diagenesis was set equal to +10‰ [72,73]. In addition, we plotted the $\delta^{18}O$–Cl^- path of a fluid experiencing smectite–illite transformation, assuming that the water liberated during this reaction has a $\delta^{18}O$ between 7.5‰ and 10‰ [64,74], with the following two end member mixing model:

$$\delta^{18}O_w([Cl^-]) = \delta^{18}O_{wi}\frac{[Cl^-]}{[Cl^-]_i} + \delta^{18}O_{sm}\left(1 - \frac{[Cl^-]}{[Cl^-]_i}\right) \quad (7)$$

where $\delta^{18}O_{sm}$ is the $\delta^{18}O$ of water liberated from smectite (7.5–10‰) and $[Cl^-]_i$ is the chloride concentration of the starting fluid (355 mM). Thus, among the processes that increase salinity, evaporation leads to an increase in the $\delta^{18}O$ of fluids, while gas hydrate formation and ash alteration lead to a decrease in fluid $\delta^{18}O$. The smectite–illite transformation, instead, freshens pore water and results in an increase in $\delta^{18}O$.

The Dvurechenskii $\delta^{18}O$–Cl^- data do not plot on any one of the model curves, but lie between the evaporation and the ash diagenesis and gas hydrate formation curves (Fig. 7). This suggests that a combination of processes produces the $\delta^{18}O$–Cl^- signature of the Dvurechenskii fluids. Elevated chlorinities associated with volcanic ash alteration have been observed in sedimentary basins where volcanic deposits are abundant [58,75]. Drilling during DSDP Leg 42A, however, showed that volcanic ashes or basaltic rocks are very scarce in Black Sea sediments. Notwithstanding, Black Sea sediments are undergoing intense silicate weathering driven by the dissolution of detrital silicates [59]. Since detrital silicates make up up to 60 wt.% of Black Sea sediments [76], the potential for a significant chlorinity increase exists. Recent results from ODP Leg 204 show that an elevated pore water chlorinity (~900 mM) is associated with rapidly forming gas hydrates, if methane is transported upwards as gas bubbles [77]. In that setting, methane bubble transport results in elevated rates of gas hydrate formation which are necessary to produce high Cl^- concentrations through the ion exclusion effect. Acoustic flares attributed to intense methane venting at the DMV have been observed recently during echosounder surveys (Artemov, personal communication), suggesting that also at the DMV gas hydrate formation could increase pore water chlorinity. Finally, it is possible that Black Sea waters prior to burial were more saline than modern Black Sea waters and that part of the salinity of the DMV fluids was produced prior to burial during evaporation. However, since the smectite–illite transformation increases the $\delta^{18}O$ of fluids (Fig. 7), evaporation likely is not the sole water-consuming process, because the resulting fluid would be significantly more enriched in ^{18}O than the Dvurechenskii fluid. The most probable scenario is that most of the salinity anomaly of the Dvurechenskii fluids was acquired through diagenesis (silicate alteration and possibly gas hydrate formation), rather than through evaporation.

5.3. Benthic chemical fluxes and relevance to geochemical cycles

Dissolved B and Li, I and DIN behave conservatively in surficial sediments of the cold seep environment. Thus, the fluxes of these species from the DMV can be calculated by multiplying the total water flux from the DMV by their concentration at depth (see below). The distribution of Ba^{2+} and Sr^{2+} in cold seep sediments, instead, is affected by the precipitation of strontian barite ($(Ba,Sr)SO_4$) near the seafloor [24,27]. In this process, dissolved Ba and Sr rising with the seeping fluids react with downward diffusing sulphate either in the sediment, to form dispersed crystals and crusts, or in the water column, to form barite chimneys [24,78]. Ba^{2+} profiles in short cores from the DMV show Ba^{2+} depletions in the top 5 cm of sediments, in

correspondence to the sulphate penetration depth (Fig. 4), indicating ongoing barite precipitation in surface sediments of the DMV. At the cold seeps of the Derugin basin in the Sea of Okhotsk, where seeping fluids contain 2 mM of dissolved barium, barium escapes into the water column only at seepage rates greater than ~50 cm year^{-1}. Thus, at the conditions prevailing at the DMV sites (seepage rate of 25 cm year^{-1} and [Ba] ~0.6 mM) the barium dissolved in the rising fluids is consumed completely in the sediment by barite precipitation [27] and no significant benthic barium flux is expected above the DMV. The Sr^{2+} profile in the surface sediments of the DMV does not show evidence of being affected by consumption processes. This is probably so because the barite Sr content is relatively low (~4 wt.%; [28,78]). Thus, precipitation of barite in the shallow sediments of the DMV likely has a small effect on benthic Sr fluxes. We thus consider that the benthic Sr flux calculated as the product of the water flux and the Sr concentration in the DMV fluids is a reliable maximum estimate.

The fluid flux from the DMV is estimated by multiplying the area of the DMV crater, obtained from Fig. 3 (≈ 0.62 km^2), by the average of the three seepage rates obtained by modelling the Cl^- profile (16 cm year^{-1}) and by the average porosity (0.95) in the upper sediment layer of the three MIC cores. This results in a total water flux from the DMV of 9.4×10^{-5} km^3 year^{-1} (Table 4). The fluid discharge from the DMV is more than 10^6 times smaller than the Danube river flux and the water flux into the Black Sea from the Bosporus (Table 4), which account for the largest part of the water input to the Black Sea [79]. Li, B, Sr and DIN fluxes from the DMV are ~10^2 to 10^3 times smaller than those from the Danube River and ~10^5 to 10^6 times smaller than the input fluxes from the Mediterranean through the Bosporus (Table 4). Thus, fluid expulsion from the DMV likely has a negligible effect on Black Sea geochemical cycles of Li, B, Sr and DIN. Fluxes of I from the DMV are ~10^3 times smaller than the input flux from the Bosporus (Table 4). About 40 mud volcanoes are known from the Sorokin Trough and about 10 in the central Black Sea (Michael Ivanov, personal communication). Should these mud volcanoes share the rather sluggish activity of DMV, cold seepage would represent ~5% of the I flux from the Bosporus. Thus, mud volcanism is a potentially significant source in the Black Sea I geochemical cycle. This is particularly so because, at present, the DMV is in a dormant phase where only dewatering and degassing into the bottom water occur. Very likely, during active mud eruption phases, water and elemental fluxes are probably much higher. In addition, large regions of the continental margins and of the deep Black Sea remain unexplored to date, and future research may reveal the presence of more mud volcanoes. Thus, we consider our flux estimates to be conservative.

We can use our estimated fluxes of Li, B, Sr, I and DIN from the DMV to obtain a very rough estimate of

Table 4
Comparison between estimated water, Li, Ba, Sr, B, I and dissolved inorganic nitrogen (DIN) fluxes from the DMV and the same fluxes from the Danube River and the Bosporus

	DMV flux	Danube River flux	Mediterranean input flux
[Li] (mM)	1.50[a]	$2.15^{b}\times10^{-4}$	0.026^{c}
[Ba] (mM)	0.57[a]	$3–4.5^{d}\times10^{-4}$	$8.7^{c}\times10^{-8}$
[Sr] (mM)	0.79[a]	$2–3^{e}\times10^{-3}$	$9.2^{c}\times10^{-2}$
[B] (mM)	2.17[a]	$0.1–18.6^{f}\times10^{-3}$	0.42^{c}
[DIN] (mM)	22[a]	$\sim0.01^{e}$	0.6^{c}
[I] (mM)	0.4[a]	$4^{g}\times10^{-5}$	$4.8^{c}\times10^{-4}$
Water flux (km^3 year^{-1})	9.4×10^{-5}	203^{h}	312^{i}
Li flux (mol year^{-1})	1.4×10^{5}	$5^{j}\times10^{7}$	$8.1^{k}\times10^{9}$
Ba flux (mol year^{-1})	0	$6.9–10.4^{j}\times10^{7}$	$2.7^{k}\times10^{7}$
Sr flux (mol year^{-1})	7.4×10^{4}	$4.6–6.9^{j}\times10^{8}$	$2.9^{k}\times10^{10}$
B flux (mol year^{-1})	2×10^{5}	$0.24–4.3^{j}\times10^{8}$	$1.3^{k}\times10^{11}$
DIN flux (mol year^{-1})	2.1×10^{6}	$2.3^{j}\times10^{9}$	$1.9^{k}\times10^{11}$
I flux (mol year^{-1})	3.8×10^{4}	$1.4^{l}\times10^{7}$	$7.5^{m}\times10^{7}$

[a] Average concentrations from the deepest samples in the DMV long cores.
[b] Mean of major world rivers [80].
[c] Quinby-Hunt and Turekian [86].
[d] Kenison-Falkner et al. [81].
[e] Pawellek et al. [82].
[f] Lemarchand et al. [15].
[g] Truesdale et al. [83].
[h] Berner and Berner [84].
[i] Unulata et al. [87].
[j] Calculated from the Danube river discharge and the Danube River composition.
[k] Calculated from mean ocean chemistry [86]) and the water input flux from the Bosporus [87].
[l] Calculated from the total riverine water discharge into the Black Sea [85] and the mean I concentration of these rivers [83].
[m] Luther and Campell [88].

the global flux of these elements from submarine mud volcanoes. The estimated number of submarine mud volcanoes is 10^3–10^5 [34]. Supposing that all mud volcanoes are active and share the activity of the DMV, we obtain global fluxes of Li, B and Sr which range from 100 times smaller to the same order of magnitude of the total inputs to the ocean of these elements (Table 5). The global mud volcano DIN flux, instead, is 10^2 to 10^4 times smaller than the total inputs of DIN to the ocean (Table 5). The global cold seep Li and B fluxes have been estimated by You et al. [22,23] to be equal to $0.02–0.1\times10^{10}$ and 0.2×10^{10} mol year^{-1}, respectively, based on the concentration of Li and B in accretionary complex sediments ([Li]=200–1000 μM; [B]=2 mM; [2,22,23]) and on the total water flux from convergent margins (1 km^3; [29]). Our maximum estimates of the global Li and B fluxes, based on the existence of 10^5 mud volcanoes worldwide, are roughly one order of magnitude greater than those of You et al. [22,23], indicating that fluid expulsion at mud volcanoes could play an important role in the global cycles of these species, as previously suggested by Kopf and Deyhle [25] for B. The estimated global mud volcano flux of I is the same order of magnitude of the riverine input (Table 5), confirming that sediment–ocean I transport at convergent margins could play an important role in the marine I cycle [21]. The chemistry of fluids expelled from other mud volcanoes, however, may be different from that of the DMV fluids, as well as flow rates and water fluxes may differ considerably. Thus, we have produced estimates of the global mud volcano fluxes of Li, Sr and DIN using data from the Atalante mud volcano on the toe of the Barbados accretionary prism [11,31]. Because both the concentrations of these species and the water flux are smaller at the Atalante mud volcano, compared to those at the DMV, the resulting global fluxes are roughly one order of magnitude smaller than those calculated considering fluxes at the DMV. Although this exercise shows how poorly constrained the global mud volcano chemical fluxes are, it also confirms that fluid expulsion at mud volcanoes may play a role in the global geochemical cycles of some chemical species.

6. Conclusion

The Dvurechenskii mud volcano expels high-salinity fluids which were formed during burial by diagenetic processes. The Ca^{2+} enrichment and the K^+, Mg^{2+}, and ^{18}O depletion of fluids are consistent with the alteration of silicate phases (volcanic ashes and/or detrital silicates). The Li/Mg geothermometer indicates that these reactions took place starting from a temperature of roughly 100 °C, which is encountered at a depth of ~3 km in the sedimentary pile of the Sorokin Trough. This temperature estimate is consistent with the enrichment of Li and B in the diagenetic fluids and falls in the field where the smecite–illite transformation takes place. In the shallow subsurface, gas hydrate formation probably contributes to enhance the salinity of the seeping

Table 5
Comparison between estimated water, Li, Ba, Sr, B, I and dissolved inorganic nitrogen (DIN) fluxes from the DMV, estimated global mud volcano fluxes and the input fluxes of these elements to the global ocean

	DMV flux	Global MV flux (DMV)[a]	Global MV flux (ATL)[b]	Inputs to ocean
Li flux (mol year^{-1})	1.4×10^5	~10^8–10^{10}	~10^7–10^9	$2.28–4.46^{c}\times10^{10}$
Ba flux (mol year^{-1})	0	0	–	–
Sr flux (mol year^{-1})	7.4×10^4	~10^8–10^{10}	~10^7–10^9	$3.86^{d}\times10^{10}$
B flux (mol year^{-1})	2×10^5	~10^8–10^{10}	–	$4.4^{e}\times10^{10}$
I flux (mol year^{-1})	3.8×10^4	~10^7–10^9	–	$9.7^{f}\times10^8$
DIN flux (mol year^{-1})	2.1×10^6	~10^9–10^{11}	~10^8–10^{10}	$7.4–8.8^{g}\times10^{12}$

[a] (a) Calculated based on the DMV fluxes and the existence of 10^3–10^5 mud volcanoes worldwide [33].
[b] Calculated based on the Atalante mud volcano fluxes [11,31] and the existence of 10^3–10^5 mud volcanoes worldwide [33].
[c] Zhang et al. [9].
[d] Wallmann [20].
[e] Lemarchand et al. [15].
[f] Muramatsu et al. [21].
[g] Berner and Berner [84].

fluids. Fluids are released to bottom waters at an average rate of 16 cm $year^{-1}$, producing a total water discharge of 9.4×10^{-5} km^3 $year^{-1}$. Seepage rates are greatest at the centre of the mud volcano (25 cm $year^{-1}$) and decline towards the edge of the active summit area (8 cm $year^{-1}$). A significant benthic flux of I is produced, which could represent ~5% of the inputs of I to the Black Sea if the 50 known mud volcanoes of the Black Sea share the rather sluggish activity of the DMV. Fluxes of other species are either negligible (Li^+, Sr^{2+}, B and DIN) or absent (Ba^{2+} in the rising fluids is consumed completely by barite precipitation processes in the sediments). Mud volcanism may play a role in the global marine cycles of Li, Sr, B, I and DIN if current estimates of mud volcano abundance are correct.

Acknowledgements

The captains and crew members of the research vessel *Meteor* provided helpful assistance at sea; their work is greatly appreciated. A special thanks goes to Bettina Domeyer, Anke Bleyer and Kristin Naß for having carried out the analytical work on board the *Meteor* and at the shore-based GEOMAR laboratories. Funding for this study was provided by the Deutsche Forschungsgemeinschaft (DFG) grant Sn 114/11-1. The study was also supported by grant 03G0566A (collaborative project OMEGA) of the Federal Ministry of Education and Research (BMBF, Bonn). This is publication GEOTHECH no. 72 of the GEOTECHNOLOGIEN program of the BMBF and the DFG. We are grateful to Marta Torres and Jonathan Martin for having critically reviewed this manuscript.

References

[1] B. Carson, E. Suess, J.C. Strasser, Fluid flow and mass flux determinations at vent sites on the Cascadia margin accretionary prism, J. Geophys. Res. 95 (B6) (1990) 8891–8897.

[2] J.B. Martin, M. Kastner, H. Elderfield, Lithium: sources in pore fluids of Peru slope sediments and implications for oceanic fluxes, Mar. Geol. 102 (1991) 281–292.

[3] E. Suess, M. Torres, G. Bohrmann, R.W. Collier, J. Greinert, P. Linke, G. Rheder, A. Trehu, K. Wallmann, G. Winkler, E. Zuleger, Gas hydrate destabilisation: enhanced dewatering, benthic material turnover and large methane plumes at the Cascadia convergent margin, Earth Planet. Sci. Lett. 170 (1999) 1–15.

[4] G.W. Claypool, I.R. Kaplan, The origin and distribution of methane in marine sediments, in: I.R. Kaplan (Ed.), Natural Gases in Marine Sediments, Plenum, New York, 1974, pp. 99–139.

[5] J. McManus, W.M. Berelson, G.P. Klinkhammer, K.S. Johnson, K.H. Coale, R.F. Anderson, N. Kumar, D.J. Burdige, D.E. Hammond, H.J. Brumsack, D.C. McCorkle, A. Rushdi, Geochemistry of barium in marine sediments: implications for its use as a paleoproxy, Geochim. Cosmochim. Acta 62 (21/22) (1998) 3453–3473.

[6] M.E. Torres, H.J. Brumsack, G. Bohrmann, K.C. Emeis, Barite fronts in continental margin sediments: a new look at barium remobilization in the zone of sulfate reduction and formation of heavy barites in diagenetic fronts, Chem. Geol. 127 (1996) 125–139.

[7] L.H. Chan, J.M. Gieskes, C.F. You, J.M. Edmond, Lithium isotope geochemistry of sediments and hydrothermal fluids of the Guaymas Basin, Gulf of California, Geochim. Cosmochim. Acta 58 (1994) 4443–4454.

[8] C.F. You, P.R. Castillo, J.M. Gieskes, L.H. Chan, A.J. Spivack, Trace element behavior in hydrothermal experiments: implications for fluid processes at shallow depths in subduction zones, Earth Planet. Sci. Lett. 140 (1996) 41–52.

[9] L. Zhang, L.-H. Chan, J.M. Gieskes, Lithium isotope geochemistry of pore waters from Ocean Drilling Program Sites 918 and 919, Irminger Basin, Geochim. Cosmochim. Acta 62 (14) (1998) 2437–2450.

[10] P. Stoffyn-Egli, F.T. Mackenzie, Mass balance of dissolved lithium in the ocean, Geochim. Cosmochim. Acta 48 (1984) 859–872.

[11] J.B. Martin, M. Kastner, Chemical and isotopic evidences for sources of fluids in a mud volcano field seaward of the Barbados accretionary wedge, J. Geophys. Res. 101 (1996) 20325–20345.

[12] L.H. Chan, J.M. Edmond, G. Thompson, K. Gillis, Lithium isotopic composition of submarine basalts: implications for the lithium cycles in the oceans, Earth Planet. Sci. Lett. 108 (1992) 151–160.

[13] L.H. Chan, J.M. Edmond, G. Thompson, A lithium isotope study of hot springs and metabasalts from mid-oceanic ridge hydrothermal systems, J. Geophys. Res. 98 (1993) 9653–9659.

[14] H.J. Smith, A.J. Spivack, H. Staudigel, H. Hart, The boron isotope composition of altered oceanic crust, Chem. Geol. 126 (1995) 119–135.

[15] D. Lemarchand, J. Gaillardet, E. Lewin, C.J. Allègre, Boron isotope systematics in large rivers: implications for the marine boron budget and paleo-pH reconstruction over the Cenozoic, Chem. Geol. 190 (2002) 123–140.

[16] B. Schmitz, Barium, equatorial high productivity, and the wandering of the Indian continent, Paleoceanography 2 (1987) 63–77.

[17] G.B. Shimmield, N.B. Price, A.A. Kahn, The use of Th-230 and Ba as indicators of paleoproductivity over a 300 Kyr time

scale—evidence from the Arabian Sea, Chem. Geol. 70 (1988) 112.
[18] J. Dymond, E. Suess, M. Lyle, Barium in deep-sea sediments: a geochemiocal proxy for paleoproductivity, Paleoceanography 7 (1992) 163–181.
[19] D.W. Lea, Constraints on the alkalinity and circulation of glacial circumpolar deep water from benthic foraminiferal barium, Glob. Biogeochem. Cycles 7 (1993) 695–710.
[20] K. Wallmann, Controls on the Cretaceous and Cenozoic evolution of seawater composition, atmospheric CO_2 and climate, Geochim. Cosmochim. Acta 65 (18) (2001) 3005–3025.
[21] Y. Muramatsu, U. Fehn, S. Yoshida, Recycling of iodide in fore-arc areas: evidence from the iodine brines in Chiba, Japan, Earth Planet. Sci. Lett. 192 (2001) 583–593.
[22] C.F. You, A.J. Spivack, J.H. Smith, J.M. Gieskes, Mobilization of boron in convergent margins: implications for the boron geochemical cycle, Geology 21 (1993) 207–210.
[23] C.F. You, A.J. Spivack, J.M. Gieskes, R. Rosenbauer, J.L. Bishoff, Experimental study of boron geochemistry: implications for fluid processes in subduction zones, Geochim. Cosmochim. Acta 59 (12) (1995) 2435–2442.
[24] M.E. Torres, G. Bohrmann, E. Suess, Authigenic barites and fluxes of barium associated with fluid seeps in the Peru subduction zone, Earth Planet. Sci. Lett. 144 (1996) 469–481.
[25] A. Kopf, A. Deyhle, Back to the roots: boron geochemistry of mud volcanoes and its implications for mobilization depth and global B cycling, Chem. Geol. 192 (2002) 195–210.
[26] G.R. Dickens, T. Fewless, E. Thomas, T.J. Bralower, Excess barite accumulation during the Paleocene–Eocene thermal maximum: massive input of dissolved barium from seafloor gas hydrate reservoirs, in: S.L. Wing, P.D. Gingerrich, B. Schmitz, E. Thomas (Eds.), Causes and Consequences of Globally Warm Climates in the Early Paleogene, Boulder, Colorado, Geological Society of America Special Paper, vol. 369, 2003, pp. 11–23.
[27] G. Aloisi, K. Wallmann, S.M. Bollwerk, A. Derkachev, G. Bohrmann, E. Suess, The effect of dissolved barium on biogeochemical processes at cold seeps, Geochim. Cosmochim. Acta 68 (8) (2004) 1735–1748.
[28] M.E. Torres, J. McManus, H. Chih-An, Fluid seepage along the San Clemente Fault scarp: basin-wide impact on barium cycling, Earth Planet. Sci. Lett. 203 (2002) 181–194.
[29] M. Kastner, Fluids in convergent margins: what do we know about their composition, origin, role in diagenesis and importance for oceanic chemical fluxes? Philos. Trans. R. Soc. Lond. Ser. A 355 (1991) 243–259.
[30] R. Von Huene, D.W. Scholl, Observations at convergent margins concerning sediment subduction, subduction erosion, and the growth of continental crust, Rev. Geophys. 29 (3) (1991) 279–316.
[31] P. Henry, X. Le Pichon, S. Lallemant, S. Lance, J.B. Martin, J.-P. Foucher, A. Fiala-Médioni, F. Rostek, N. Guilhaumou, V. Pranal, M. Castrec, Fluid flow in and around a mud volcano field seaward of the Barbados accretionary wedge: results from Manon cruise, J. Geophys. Res. 101 (B9) (1996) 20297–20323.
[32] P. Henry, S. Lallemant, K. Nakamura, U. Tsunogai, S. Mazzotti, K. Kobayashi, Surface expression of fluid venting at the toe of the Nankai wedge and implications for flow paths, Mar. Geol. 18 (2002) 119–143.
[33] A. Kopf, D. Klaeschen, J. Mascle, Extreme efficiency of mud volcanism in dewatering accretionary prisms, Earth Planet. Sci. Lett. 189 (2001) 295–313.
[34] A.V. Milkov, Worldwide distribution of submarine mud volcanoes and associated gas hydrates, Mar. Geol. 167 (2000) 29–42.
[35] M. Drews, K. Wallmann, G. Aloisi, G. Bohrmann, Fluid expulsion from the Dvurechenskii mud volcano (Black Sea): Part II. Methane fluxes and their relevance to the Black Sea methane cycle, submitted for publication to Earth Planet. Sci. Lett.
[36] D.A. Tugolesov, A.S. Gorshov, L.B. Meisner, V.V. Soloviev, E.M. Khakhalev, Tectonics of Mezo-Kainozoic Deposits of the Black Sea Basin, Nedra, Moscow, 1985.
[37] M.K. Ivanov, A.F. Limonov, J.M. Woodside, Extensive deep fluid flux through the sea floor on the Crimean continental margin (Black Sea), in: J.-P. Henriet, J. Mienert (Eds.), Gas Hydrates: Relevance to World Margin Stability and Climate Change, Spec. Publ. - Geol. Soc. Lond., vol. 137, 1998, pp. 195–213.
[38] J.M. Woodside, M.K. Ivanov, A.F. Limonov, Neotectonics and fluid flow through seafloor sediments in the Eastern Mediterranean and Black Sea—Part I and II, IOC Technical Series No. 48, UNESCO (1997).
[39] G. Bohrmann, S. Schenck, cruise participants, RV METEOR Cruise Report M52/1 MARGASCH, GEOMAR Report No. 108, 2002, pp. 191.
[40] G. Bohrmann, M.K. Ivanov, J.-P. Foucher, V. Spiess, J. Bialas, J. Greinert, W. Weinrebe, F. Abegg, G. Aloisi, Y. Artemov, V. Blinova, A. Broser, M. Drews, F. Heidersdorf, I. Klaucke, S. Krastel, T. Leder, I. Polikarpov, M. Saburova, R. Seifert, A. Volkonskaya, M. Zillmer, Mud volcanoes and gas hydrates in the Black Sea—new data from Dvurechenskii and Odessa mud volcanoes, Geo-Mar. Lett. (2003).
[41] S. Krastel, V. Spiess, M. Ivanov, W. Weinrebe, G. Bohrmann, P. Shashkin, F. Heidersdorf, Acoustic investigations of mud volcanoes in the Sorokin Trough, Black Sea, Geo-Mar. Lett. (2003).
[42] M.B. Cita, E. Erba, R. Lucchi, M. Pott, R. van der Meer, L. Nieto, Stratigraphy and sedimentation in the Mediterranean Ridge diapiric belt, Mar. Geol. 132 (1996) 131–150.
[43] K.M. Brown, The nature and hydrogeologic significance of mud diapirs and diatremes for accretionary systems, J. Geophys. Res. 95 (B6) (1990) 8969–8982.
[44] K. Grasshoff, M. Ehrhardt, K. Kremling, Methods of Seawater Analysis, 2nd ed., Verlag Chemie, Weinheim, 1983, p. 419.
[45] V.N. Ivanenkov, Yu.I. Lyakhin, Determination of total alkalinity in seawater, in: O.K. Bordovsky, V.N. Ivanenkov (Eds.), Methods of Hydrochemical Investigations in the Ocean, Nauka Publ. House, Moscow, 1978, pp. 110–114, in Russian.
[46] A.D. Dickson, pH buffers for sea water media based on the total hydrogen ion concentration scale, Deep-Sea Res. I 40 (1993) 107–118.

[47] R. Luff, K. Wallmann, Fluid flow, methane fluxes, carbonate precipitation and biogeochemical turnover in gas hydrate-bearing sediments at Hydrate Ridge, Cascadia Margin: numerical modeling and mass balances, Geochim. Cosmochim. Acta 67 (2003) 3403–3421.

[48] R. Berner, Early Diagenesis: A Theoretical Approach, Princeton Series in Geochemistry, Princeton Univ. Press, Princeton, NJ, 1980.

[49] B.P. Boudreau, The diffusive tortuosity of fine-grained unilithified sediments, Geochim. Cosmochim. Acta 60 (16) (1996) 3139–3142.

[50] P. Linke, E. Suess, M. Torres, V. Martens, W.D. Rugh, W. Ziebis, L.D. Kulm, In situ measurements of fluid flow from cold seeps at active continental margins, Deep-Sea Res. I 41 (4) (1994) 721–739.

[51] J.C. Fontes, J.M. Matray, Geochemistry and origin of formation brines from the Paris Basin, France: 1. Brines associated with Triassic salts, Chem. Geol. 109 (1993) 149–175.

[52] B.B. Jørgensen, Mineralization of organic matter in the seabed—the role of sulfate reduction, Nature 296 (1982) 643–645.

[53] J.B. Martin, J.M. Gieskes, M. Torres, M. Kastner, Bromide and iodine in Peru margin sediments and pore fluids: implication for fluid origin, Geochim. Cosmochim. Acta 57 (1993) 4377–4389.

[54] P.A. Baker, J.M. Gieskes, H. Elderfield, Diagenesis of carbonates in deep-sea sediments—evidence from Sr/Ca ratios and interstitial dissolved Sr^{2+} data, Sediment. Petrolog. 52 (1982) 71–82.

[55] K. Averyt, A. Paytan, Empirical partition coefficients for Sr and Ca in marine barite: implications for reconstructing seawater Sr and Ca concentrations, Geochem., Geophys., Geosys. 4 (5) (2003) 1–14.

[56] W.E. Seyfried, D.R. Janecky, M.J. Mottl, Alteration of the oceanic crust: implications for geochemical cycles of lithium and boron, Geochim. Cosmochim. Acta 48 (1984) 557–569.

[57] J.M. Gieskes, J.R. Lawrence, Alteration of volcanic matter in deep-sea sediments: evidence form the chemical composition of interstitial waters from deep sea drilling cores, Geochim. Cosmochim. Acta 45 (1981) 1687–1703.

[58] P.K. Egeberg, Scientific Party of Leg 113, Unusual composition of pore water found in the Izu-Bonin fore-arc sedimentary basin, Nature 344 (1990) 215–218.

[59] G. Aloisi, K. Wallmann, M. Drews, G. Bohrmann, Evidence for the submarine weathering of silicate minerals in Black Sea sediments: possible implications for the marine Li and B cycles, Geochem., Geophys., Geosys. 5 (4) (2004).

[60] A. Deyhle, A. Kopf, Strong B enrichment and anomalous $\delta^{11}B$ in pore fluids from the Japan Trench forearc, Mar. Geol. 183 (2002) 1–15.

[61] T. Ishikawa, E. Nakamura, Boron isotope systematics of marine sediments, Earth Planet. Sci. Lett. 117 (1993) 567–580.

[62] L.-H. Chan, M. Kastner, Lithium isotopic compositios of pore fluids and sediments in the Costa Rice subduction zone: implications for fluid processes and sediment contribution to the arc volcanoes, Earth Planet. Sci. Lett. 183 (2000) 275–290.

[63] Y.K. Kharaka, R.H. Mariner, Chemical geothermometers and their applications to formation waters form sedimentary basins, in: N.D. Naesser, T.H. McCulloh (Eds.), Thermal History of Sedimentary Basins: Methods and Case Histories, Springer-Verlag, New York, 1989, pp. 99–117.

[64] C. Hensen, K. Wallmann, M. Schmidt, C.R. Raniero, E. Suess, Fluid expulsion related to mud extrusion off Costa Rica—a window to the subducting slab, Geology 32 (3) (2004) 201–204.

[65] K.M. Brown, D.M. Saffer, B.A. Bekins, Smectite diagenesis, pore-water freshening, and fluid flow at the toe of the Nankai wedge, Earth Planet. Sci. Lett. 194 (2001) 97–109.

[66] G.J. De Lange, J.J. Middelburg, C.H. Van der Weijden, G. Catalano, G.W. Luther, D.J. Hydes, J.R.W. Woittiez, G.P. Klinkhammer, Composition of anoxic hypersaline brines in the Tyro and Bannock Basins, eastern Mediterranean, Mar. Chem. 31 (1990) 63–88.

[67] A. Vengosh, A. Starinsky, Relics of evaporated sea water in deep basins of the eastern Mediterranean, Mar. Geol. 115 (1993) 15–19.

[68] E. Suess, G. Bohrmann, D. Rickert, A. Eisenhauer, M.J. Whiticar, Vorkommen, Gefüge und Zusammensetzung von oberflächennahen Gashydraten vom Hydrat Rüken (Cascadia Akkretionszone). Deutsche Forschungsgemeinschaft, ODP-Kolloquium Jena (2000) p. 77 [Occurrence, fabric and conposition of hydrates in near-surface sediments of the Cascadia Margin, Eos Trans. 80 (46), 1999, p. F511].

[69] R. Hesse, Pore water anomalies of submarine gas-hydrate zones as tool to asses hydrate abundance and distribution in the subsurface. What have we learned in the past decade? Earth Planet. Sci. Lett. 61 (2003) 149–179.

[70] I. Friedman, R. O'Neil, Compilation of stable isotope fractionation factors of geochemical interest, in: M. Fleischer (Ed.), Data of Geochemistry (6th edition), U.S. Geol. Surv. Prof. Paper, 1977, 440KK.

[71] R. Matsumoto, W.S. Borowski, Gas hydrate estimates from newly determined oxygen isotopic fractionation ($\alpha_{GH\text{-}IW}$) and $\delta^{18}O$ anomalies of the interstitial waters: ODP Leg 164, Blake Ridge, in: C.K. Paull, R. Matsumoto, P.J. Wallace, et al., (Eds.), Proc. Ocean Drill. Program Sci. Results, vol. 164, 2000, pp. 59–66.

[72] K. Muehlenbachs, R.N. Clayton, Oxygen isotope composition of the oceanic crust and its bearing on seawater, J. Geophys. Res. 81 (1976) 4365–4369.

[73] C. Lecuyer, P. Allemand, Modelling of the oxygen isotope evolution of seawater: implications for the climate interpretation of the $\delta^{18}O$ of marine sediments, Geochim. Cosmochim. Acta 63 (3/4) (1999) 351–361.

[74] A. Dählmann, G.J. De Lange, Fluid–sediment interactions at eastern Mediterranean mud volcanoes: a stable isotope study from ODP Leg 160, Earth Planet. Sci. Lett. 212 (2003) 377–391.

[75] J.B. Martin, Diagenesis and hydrology at the New Hebridies forearc and Aoba basin, Proc. Ocean Drill. Program Sci. Results 134 (1994) 109–130.

[76] F.T. Manheim, D.M. Schug, Interstitial waters of Black Sea cores, Initial Rep. Deep Sea Drill. Proj. 42 (1978) 637–651.

[77] M. Torres, K. Wallmann, A.M. Trehu, G. Bohrmenn, W. Borowski, H. Tomarec, Gas hydrate growth, methane transport, and chloride enrichment at the southern summit of Hydrate Ridge, Cascadia margin off Oregon, Earth Planet. Sci. Lett. In press (doi:10.1016/j.epsl.2004.07.029).

[78] J. Greinert, S.M. Bollwerk, A. Derkachev, G. Bohrmann, E. Suess, Massive barite deposits and carbonate mineralization in the Derugin Basin, Sea of Okhotsk: precipitation processes at cold seep sites, Earth Planet. Sci. Lett. 203 (2002) 165–180.

[79] E. Özsoy, Ü. Ünlüata, Oceanography of the Black Sea: a review of some recent results, Earth-Sci. Rev. 42 (1997) 231–272.

[80] Y. Huh, L.-H. Chan, L. Zhang, J.M. Edmond, Lithium and its isotopes in major world rivers: implications for weathering and the oceanic budget, Geochim. Cosmochim. Acta 62 (12) (1998) 2039–2051.

[81] K. Kenison-Falkner, D.J. O'Neill, J.F. Todd, W.S. Moore, J.M. Edmond, Depletion of barium and radium-226 in Black Sea surface waters over the past thirty years, Nature 350 (1991) 491–494.

[82] F. Pawellek, F. Frauenstein, J. Veizer, Hydrochemistry and isotope geochemistry of the upper Danube River, Geochim. Cosmochim. Acta 66 (2002) 3839–3854.

[83] V.W. Truesdale, S.F. Watts, A.R. Rendell, On the possibility of iodide oxidation in the near-surface of the Black Sea and its implications to iodine in the general ocean, Deep-Sea Res. I 48 (2001) 2397–2412.

[84] E.K. Berner, R. Berner, Global Environment: Water, Air, and Geochemical Cycles, Prentice Hall, Upper Saddle River, NJ, 1996, 376 pp.

[85] P.K. Swart, The oxygen and hydrogen isotopic composition of the Black Sea, Deep-Sea Res. II 38 (1991) 761–772.

[86] M.S. Quinby-Hunt, K.K. Turekian, Distribution of elements in seawater, EOS 64 (1983) 130–131.

[87] U.T. Unulata, T. Oguz, M.A. Latif, E. Ozsoy, On the physical oceanography of the Turkish Straits, in: L.J. Pratt (Ed.), The Physical Oceanography of Sea Straits, NATO ASI Ser., Deventer, The Netherlands, 1990, pp. 25–60.

[88] G.W. Luther, T. Campbell, Iodine speciation in the water column of the Black Sea, Deep-Sea Res. II 38 (1991) S875–S882.